Ultrasound in Med. & Biol., Vol. 42, No. 11, pp. 2572–2588, 2016

0301-5629/$ - see front matter

http://dx.doi.org/10.1016/j.ultrasmedbio.2016.07.002

● *Original Contribution*

IN VITRO COMPARISON OF FIVE DIFFERENT ELASTOGRAPHY SYSTEMS FOR CLINICAL APPLICATIONS, USING STRAIN AND SHEAR WAVE TECHNOLOGY

ANESA MULABECIROVIC,*† METTE VESTERHUS,*‡ ODD HELGE GILJA,*† and ROALD FLESLAND HAVRE*

*National Centre for Ultrasound in Gastroenterology, Haukeland University Hospital, N-5021 Bergen, Norway; †Institute of Clinical Medicine, University of Bergen, N-5020, Bergen, Norway; and ‡Norwegian PSC Research Center, Department of Transplantation Medicine, Division of Cancer Medicine, Surgery and Transplantation, Oslo University Hospital Rikshospitalet, Oslo, Norway

(*Received* 15 *January* 2016; *revised* 30 *June* 2016; *in final form* 2 *July* 2016)

Abstract—Several different platforms providing ultrasound elastography have emerged in recent years. In this *in vitro* study on a single tissue-mimicking phantom (CIRS Model 49), we aimed to compare the performance of quantitative elastography measurements from platforms running strain elastography and others running shear wave elastography. We evaluated five different elastography platforms using both linear and curvilinear probes. All measurements were performed in parallel by two independent investigators who recorded the elasticity quantitatively. We investigated intra- and inter-observer agreement by intra-class correlation analysis and coefficient of variation, by correlation and limits of agreement. The reproducibility of elasticity measurements was good to excellent for shear wave and strain elastography. All five elastography platforms had high intra-observer (intra-class correlation coefficient: 0.932–1.0) and inter-observer correlation (intra-class correlation coefficient: 0.845–0.996). All inclusions could be differentiated by quantitative elastography by all systems ($p < 0.001$). The use of a linear probe yielded more reproducible measurements compared with use of a convex probe in 3/4 platforms. (E-mail: roald.flesland.havre@helse-bergen.no) © **2016 The Authors. Published by Elsevier Inc. on behalf of World Federation for Ultrasound in Medicine & Biology. This is an open access article under the CC BY-NC-ND license (http://creativecommons.org/licenses/by-nc-nd/4.0/).**

Key Words: **Ultrasound elastography, Shear wave imaging, Strain imaging, Phantom.**

INTRODUCTION

Ultrasound (US) elastography is a common term for imaging techniques that aim to visualize or assess tissue elasticity by ultrasound. In the clinical application, elastography provides images or measures of what medical doctors may sense by palpation. Two main methodologies are available in clinical scanners, strain elastography (SE) and shear wave elastography (SWE), although there are several technical differences between the makers of US scanner software (Bamber et al. 2013). Both methods have proven useful for non-invasive diagnosis of tissue pathology in several organs such as breast, thyroid, liver, lymph nodes and pancreas (Bhatia et al. 2012; D'Onofrio et al. 2016; Fraquelli et al. 2007; Friedrich-Rust et al. 2016; Garra et al. 1997; Giovannini et al. 2009; Itoh et al. 2006; Janssen et al. 2007; Janssen and Papavassiliou 2014; Mei et al. 2013; Pozzi et al. 2012; Saftoiu et al. 2008; Salomon et al. 2008; Sebag et al. 2010; Sporea et al. 2012b; Tsutsumi et al. 2007; Ying et al. 2012; Zhi et al. 2007). Some studies have investigated the *in vitro* reproducibility of single platforms (Carlsen et al. 2015) or compared two or several modalities in phantom studies (Carlsen et al. 2015; Dillman et al. 2015; Franchi-Abella et al. 2013; Oudry et al. 2014; Shin et al. 2016), as well as in the livers of patients and healthy controls (Cassinotto et al. 2014; Ferraioli et al. 2012b). However, few other studies have compared the reproducibility of several different SWE platforms in a head-to-head study with strain-based elastography platforms in the same test patients in five different clinically applied US systems.

Strain elastography uses autocorrelation of the position of image lines under repeated applied stress, creating an image of local strain superimposed on the B-mode image in real time. The method is also known as quasi-static elastography because of the relatively slow compression and decompression compared with the US frame rate. For quantitative analysis, a built-in method for comparing strain in two or more user-selected areas, called the strain

Address correspondence to: Roald Flesland Havre, Department of Medicine, Haukeland University Hospital, Jonas Lies vei 49, N-5021 Bergen, Norway. E-mail: roald.flesland.havre@helse-bergen.no

ratio (SR), may be used. Because the method is applied freehand, we have no knowledge of the stress applied. For quantification, we have used the relative difference in strain:

$$\mathrm{SR} = \frac{\text{Mean strain in reference area } (B)}{\text{Mean strain in lesion } (A)} \quad (1)$$

The SR represents the elastic contrast between two areas within the insonified plane. By defining the SR as in eqn (1), any lesion harder than the reference tissue will have an SR > 1. As a consequence, a higher SR value represents increased tissue stiffness in the lesion relative to the reference tissue selected. A pre-condition in using SR as a measurement for tissue stiffness determination is that the two areas have been subject to similar stress (Cho et al. 2010; Havre et al. 2014; Itokawa et al. 2011). The tissue stiffness is measured with Young's modulus and expressed as pressure in pascals (Pa). The relationship between the local stress and the resulting strain is defined by Young's modulus (E), and it quantifies tissue stiffness.

$$E = \frac{\Delta\text{strain}}{\Delta\text{stress}} \quad (2)$$

When shear wave speed is the basis of elasticity quantification, the calculation of the shear modulus is based on two assumptions: the first is that the tissue density (ρ) is a constant and expressed in kg/m^3. The density of healthy tissue is relatively constant in the body and very close to the density of water (1000 kg/m^3):

$$\text{Shear modulus}(\mu) = \rho(c_{sw})^2 \quad (3)$$

where c_{sw} represents the shear wave speed. The other assumption is that the soft tissue behaves like an incompressible material with a Poisson ratio (ν) of ≈ 0.5.

$$\text{Shear modulus } (\mu) = \frac{\text{Elastic modulus } (E)}{2(1 + \text{Poisson ratio}[\nu])} \quad (4)$$

Using the $\nu \approx 0.5$ assumption in this equation yields the following relationship between the shear modulus (μ) and the Young's modulus (E):

$$E \approx 3\mu \quad (5)$$

The expected values for shear wave velocities are calculated as

$$c_{sw} = \sqrt{\left(\frac{E}{3\rho}\right)} \quad (6)$$

We used the values for tissue density (ρ) and Young's modulus (E) as provided by the manufacturer of the phantom.

Shear wave-based elastography systems use physical excitation of tissue, often provided by an acoustic pulse of adequate energy, to create local shear waves traveling perpendicular to the longitudinal US waves. Shear waves are transverse wave deformations and travel slower than US waves in tissue. They may be tracked by continuous US scanning so that their speed may be measured over relatively limited distances (Palmeri et al. 2005a, 2005b).

Point shear wave elastography (pSWE) on the Philips iU22 is a method that produces a quantitative measurement of tissue elasticity, but no visualization of strain or Young's modulus. Supersonic shear wave elastography (supersonic imaging [SSI]) (Bamber et al. 2013; Bercoff et al. 2004) uses a different method that enables ultrafast frame rates. SSI provides both elasticity imaging and quantification (in kPa) or shear wave speed (m/s) in a 2-D area larger than that in pSWE. A transient cone of shear waves is created by several acoustic push pulses deposited at different depths with a small time lag. This creates an expanding "acoustic cone" that can be tracked using plane US waves at high frame rates (Deffieux et al. 2009; Gennisson et al. 2010; Tanter et al. 2008).

Considering the expanding spectrum of ultrasound-based elastography systems that have evolved, we wanted to assess and compare the intra- and inter-observer reliability of several commercially available systems in a tissue-mimicking phantom. The aim of this study was to assess the repeatability of quantitative elastography measurements by five different elastography systems in a tissue-mimicking phantom with inclusions of known Young's modulus. Both linear and curvilinear US probes were used as available for elasticity imaging and/or measurement.

METHODS

The scanners and elastography software used in this study were commercially available except for one software, GE-SWE, which was unreleased at the time of data recording. The methods were approved for medical use in diagnostic ultrasonography and reported the local tissue elasticity in terms of strain or shear wave speed. Five different elastography systems were evaluated in terms of intra- and inter-observer reproducibility. Two of the systems were strain-based imaging methods: Real-time elastography (Ascendus, Hitachi Medical, Zug Switzerland) and GE Logiq E9 (GE Ultrasound, Milwaukee, IL, USA). The strain ratio, SR (Hitachi), or elasticity index, E (GE), was used for relative strain quantification. Three of the systems were based on measurement of shear wave speed as a basis for determination of tissue elasticity. These systems were pSWE (Philips

iU22 XM, Eindhoven, Netherlands), SSI (Aixplorer, Aix-en-Provence, France) and one shear-wave elastography software from GE Healthcare (Milwaukee, WI, USA) used on a GE Logiq E9 scanner.

The object for examination was a tissue-mimicking phantom (Model 049 Elasticity QA Phantom, Computerized Imaging Reference Systems Company [CIRS], Norfolk, VA, USA). The phantom is made of a polymer (Zerdine) and was individually quality assessed by the producer. The phantom had the following ultrasound properties: speed of sound in the background = 1540 ± 10 m/s, attenuation coefficient = 0.5 ± 0.05 dB/cm-MHz, density = 1.04 g/cm^3. The densities of inclusions 1–4 and the background were 1.04, 1.05, 1.06, 1.05 and 1.05 g/cm^3 (Table 1). The elasticities selected for lesions and background material were comparable to elastic contrasts found in biological tissue; however, the phantom material did not possess viscous properties similar to those of biological tissue (Browne et al. 2003). According to the producer, the standard deviation of the measurement was 5%. The phantom contained eight spherical inclusions, representing four different elasticities: 8 ± 3, 14 ± 4, 45 ± 8 and 80 ± 12 kPa in a background of 25 ± 6 kPa. Four inclusions with a diameter of 20 mm and four with a diameter of 10 mm were situated with central depths of 35 and 15 mm, respectively. For the assessment of diagnostic performance, the four largest inclusions (diameter = 20 mm) were used in this study.

A standardized circular region of interest (ROI) with diameter 15 mm was used over the inclusions for all modalities, except for point shear wave elastography (Philips iU22). A reference ROI with a diameter of 7 mm was used when the sampling areas were adjustable. Ratios between two areas were available as a mode quantification for the strain elastography systems (RTE, Hitachi, and GE-SE, GE), as illustrated in Figure 1.

Three observers (A.M., R.F.H. and M.V.) participated in the study. Only one observer (A.M.) obtained data from all scanners; R.F.H. obtained data from Hitachi, GE strain and GE-SWE and Aixplorer; and MV obtained data from the Philips iU22. The observers had varying experience in ultrasound and elastography studies: R.F.H. had 7 y of experience in ultrasound and elastography studies, M.V. had 3 y of experience in ultrasound and elastography studies and A.M. had 4 mo of experience in ultrasound and 1 mo in elastography studies. None of the observers was experienced with all of the systems at the time of data collection. R.F.H. and M.V. had individually more experience with Hitachi and Philips, respectively, than A.M. For GE and Aixplorer, the difference in experience was limited for all observers. Each observer was blinded to the others' results and independently performed measurements and collected data by scanning the phantom. Both curvilinear and linear probes provided elasticity imaging or quantification (Bamber et al. 2013). All observers used the same elastography image settings. Each image was recorded to the hard drive of the scanners and subsequently stored on an external storage device. Quantitative measurements of the elasticities were also recorded for each acquisition.

Description and settings of the elasticity imaging scanning platforms applied

Software versions and default settings are provided in the Appendix.

Supersonic shear wave elastography (SSI). This scanner provided an elasticity color map superimposed on the B-mode echogram, where *red* and *blue* indicated harder and softer tissue, respectively. The ROI could be adjusted in size and position. We compared an ROI 15 mm in diameter placed centrally within the lesion with a reference tissue ROI 7 mm in diameter (Fig. 1a). One long cine loop was recorded for each lesion, allowing the designation of 10 ROIs for quantitative analysis post-acquisition, and results were given as the median of 10 repeated measurements using kPa and shear wave speed in m/s. The probe was held still with a minimum of pressure on the phantom surface. The elasticity is directly deduced by measuring the speed of shear wave propagation (m/s), as indicated in eqn (5), and presented in an elasticity color map. The default scanner settings were applied, and scanning was performed using the probes C6-1 (curvilinear) and L10-2 (linear).

Shear wave elastography (GE Logiq E9, GE-SWE). This scanner provided an elasticity color map superimposed on the B-mode echogram. The ROI could be adjusted in size and position. One long cine loop was recorded for each lesion, allowing the designation of 10 ROIs for quantitative analysis post-acquisition,

Table 1. Expected measurements for all inclusions and background material ± 5% SD

Inclusion	Young's modulus (kPa)	Density (g/cm^3)	Expected shear wave velocity (m/s)	Expected elastic ratio
1	8 ± 3	1.04	1.60 ± 0.08	0.3 ± 0.02
2	14 ± 4	1.04	2.12 ± 0.11	0.6 ± 0.03
3	45 ± 8	1.05	3.78 ± 0.19	1.8 ± 0.09
4	80 ± 12	1.06	5.02 ± 0.25	3.2 ± 0.20
Background	25 ± 6	1.05	2.82 ± 0.14	1.0 ± 0.05

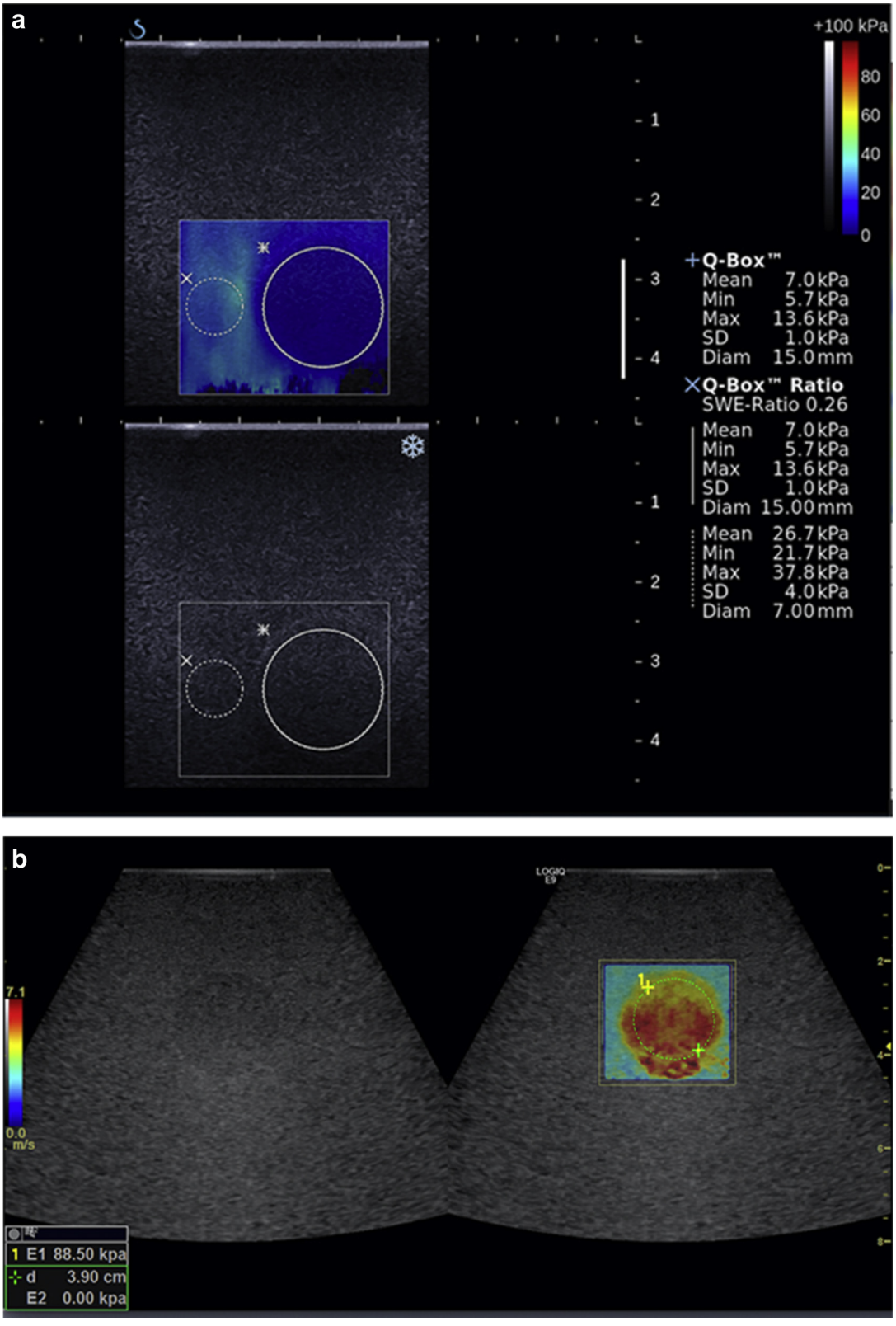

Fig. 1. Images of phantom scanning for all systems, with region of interest settings. (a) Aixplorer. (b) GE-SWE. (c) GE-SE. (d) Hitachi. (e) Philips.

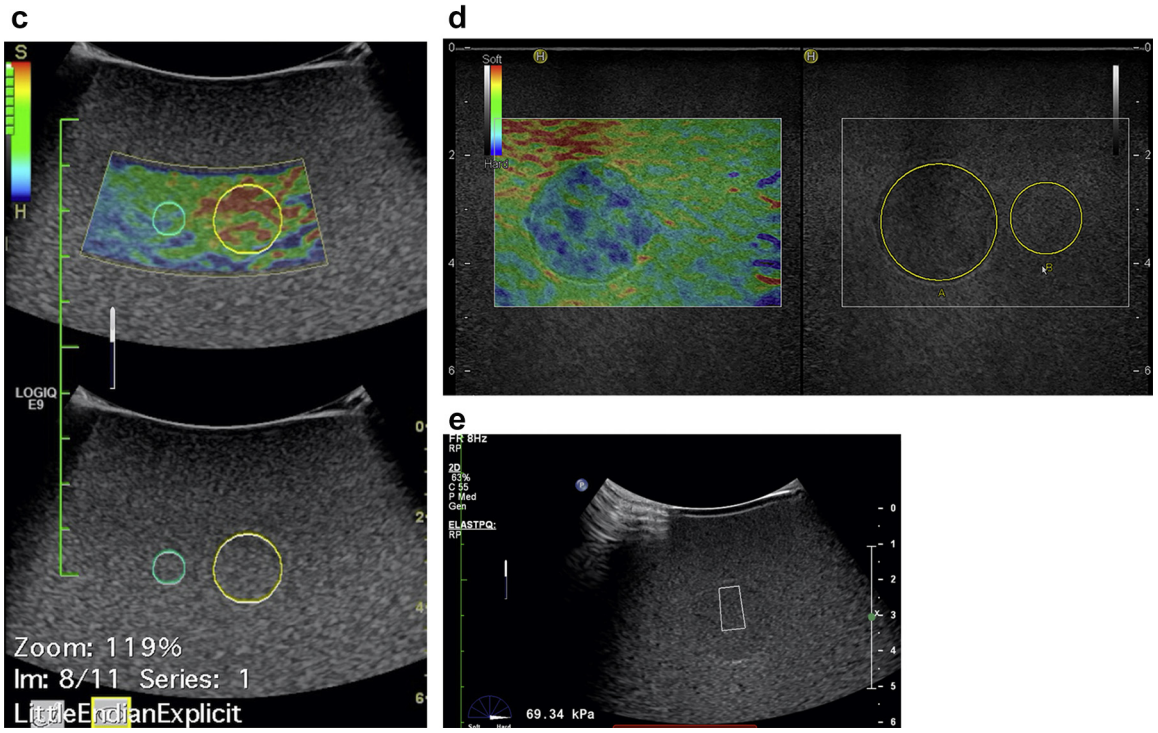

Fig. 1. (*continued*).

and results were given as the median of 10 repeated measurements (Fig. 1b). The data were recorded as elasticity using kPa and as shear wave speed in m/s. The probe was held still with a minimum of pressure on the phantom surface. The default scanner settings were applied and scanning was performed using both C6-1 (curvilinear) and 9 L (linear) probes.

Strain elastography (GE Logiq E9, GE-SE). Freehand scanning with a compression rate that provided a stable elastogram was applied to the scanner surface. A strain-based elasticity color map was provided superimposed on the B-mode image. Elasticity was reported as elasticity index (*E*), a unitless scale representing the relative strain value. The elasticity index was calculated as average strain in a user-selected circular area over the inclusion within the ROI divided by the average strain in the ROI as a whole (Fig. 1c). *E* values 0–1 indicate a softer region with higher than the average strain, whereas values >1 indicate a harder region of lower than average strain. Several elasticity ROIs could be designated during the same scanning, and we applied our standardized sample areas over inclusions and reference material. We recorded consecutive measurements within a stable cine loop and where the quality indicator displayed a green signal. Each measurement was repeated 10 times and *E* (0–6) was registered. The default scanner settings were applied and scanning was performed using both 9 L (linear) and C1-5 (curvilinear) probe.

Real-time elastography (Hitachi). Freehand scanning with a compression rate that provided a stable elastogram (80–100/min) was applied to the phantom surface. The scanner provided a strain color map in real time over a B-mode image. Calculation of SR was done on a loop sequence with adequate signal according to the strain indicator curve. Ten different SR values were calculated as mean strain in reference tissue (*B*) divided by mean strain in the inclusion (*A*) recorded from a representative cine loop of each lesion (Fig. 1d). The default RTE scanner settings were applied and scanning was performed using the L53 (linear) probe and C5-1 (curvilinear) probe.

Point shear wave elastography (Philips). This scanner provided an ROI for elasticity measurement with a fixed area (0.5 cm in the lateral direction, 1 cm in the axial direction) that could be placed freely within the field of view. The ROI was placed centrally within the inclusions (Fig. 1e). No recording of reference tissue elasticity was possible when scanning the inclusions. Instead, the background material was scanned in a separate session at the same depth as the four inclusions. Default scanner settings and a curvilinear probe (C5-1) were applied and measurements were made while the probe was held still

with minimum pressure on the phantom surface. Ten repeated acquisitions were made, and the result was given as the median of 10 individual measurements. The measurements were recorded in shear wave velocity as m/s and in kPa. This modality did not provide a strain image.

Statistical analysis

IBM SPSS Statistics Version 20 was used for all statistical analyses. Data were analyzed using descriptive statistics and one-way analysis of variance. Elasticity values are presented as median values with min–max values over 10 consecutive measurements of each inclusion. The median elasticity quantification value and interquartile range is presented for each platform in the boxplot. Intra-observer variability is provided by the coefficient of variation (CV), which is the standard deviation (SD) divided by the mean value. A low CV is equivalent to high measurement repeatability. Inter-observer reliability is presented as the inter-class correlation coefficients (ICC). High inter-observer reliability is indicated by an ICC near 1.00. Inter-observer agreement was further assessed by correlation plot analysis using Pearson's correlation coefficient (r), and differences between individual measurements are reported as limits of agreement for each of the platforms and the probes used (Bland and Altman 1999, 2007).

SPSS version 20 IBM Statistics (Armonk, New York, NY, USA) was used for statistical analysis.

RESULTS

Differentiation of inclusions

Elastography with quantification of measurements was performed on all four lesions and the background material in the tissue-mimicking phantom. In Table 2, the median elasticity values, or median strain ratios, for each of the four inclusions are given for all platforms and probes and by the individual observer as well as the pooled results. All four lesions could be significantly differentiated by their elasticity measurements using any of the five elastography methods ($p < 0.001$). The boxplots for observers A and B (Fig 2a–i) for all inclusions illustrate the median values, as well as the measurement variability, the interquartile range is represented by the vertical distribution of the box for each inclusion. In Table 3, we present the intra- and inter-observer variation based on mean values of SR or SWE as the CV and ICC. For shear wave elastography with the Philips, SSI and GE-SWE, median elasticity values were closer to the elasticity value given by the producer of the phantom for the hardest inclusion (inclusion 4) compared with the softer inclusions. This was found for both the linear and curvilinear probes. Strain elastography by GE-SE and Hitachi achieved significantly different E and SR values, respectively, for each inclusion.

Measurement variability

All systems had a pooled CV <1.0, which corresponds to low variance and high reproducibility in measurements (Table 3). Generally, variability in measurements exhibited a tendency to increase, with harder lesions yielding higher measurement values. For shear wave elastography, however, the variability was similar for the two softest lesions and for the two hardest lesions, respectively, for all three methods. For strain elastography, RTE exhibited a trend toward lower variability for the two softest lesions than for the two hardest lesions (Table 3). For GE-SE, CVs were in the ranges 0.00–0.16 for the two softest lesions and 0.05–0.19 for the two hardest lesions (Table 3). All systems exhibited high inter-observer reliability as assessed by ICC, indicated by ICCs in the ranges 0.85–1.00 for strain methods and 0.99–1.00 for shear wave methods.

Differences in repeatability by method

High repeatability in elasticity measurements was obtained for both strain elastography methods, as well as all three shear wave elastography methods. The correlation between observers A and B was excellent for all platforms, with correlation coefficients r in the range 0.937–0.997 (Fig. 3a–i). In Figure 4a–i, Bland–Altman plots illustrate the differences in individual measurements from a common mean value for both observers. A deviation of the mean from 0 on the second axis would represent a difference between the observers, and could indicate bias between observers. However, this deviation is very limited in all platforms (Fig. 4a–i). A common feature of all platforms is a tendency for larger variability for inclusions 3 and 4 compared with inclusions 1 and 2, as indicated by a larger data spread as visualized by higher boxes (IQR) in the boxplots (Fig. 2a–i) and larger spread of measurements in correlation and Bland–Altman plots (Figs. 3 and 4a–i).

Differences in repeatability by linear or curvilinear probe

For a majority of the platforms, the measurements exhibited higher variation when the curvilinear probe was used than when the linear probe was used while scanning the phantom inclusions; however, one of the strain-based platforms (RTE) exhibited larger measurement variation for the linear probe than for the curvilinear probe (Fig. 4g, h). Correlation between observers also exhibited a tendency toward higher correlation coefficients for linear probes compared with curvilinear probes for each system, except for RTE, where the correlation coefficient was higher for the curvilinear probe (Fig. 3g, h).

Table 2. Median elasticity measurements for all systems

Elastography system	Probe shape	Observer	Inclusion 1 (8 ± 3 kPa) (ER 0.3 ± 0.02)	Inclusion 2 (14 ± 4 kPa) (ER 0.66 ± 0.03)	Inclusion 3 (45 ± 8 kPa) (ER 1.8 ± 0.09)	Inclusion 4 (80 ± 12 kPa) (ER 3.2 ± 0.20)
Philips	Curvilinear	A	6.2 kPa (5.7–6.5)	11.8 kPa (10.1–13.5)	42.9 kPa (37.6–51.1)	59.5 kPa (48.4–69.3)
		B	6.3 kPa (5.6–7.4)	12.2 kPa (12.0–12.7)	39.0 kPa (35.8–46.7)	50.4 kPa (46.8–62.0)
		A + B	6.2 kPa (5.6–7.4)	12.1 kPa (10.1–13.5)	41.0 kPa (35.8–51.1)	55.5 kPa (46.8–69.3)
GE-SWE	Linear	A	7.4 kPa (7.2–7.5)	10.9 kPa (10.8–11.0)	41.9 kPa (41.3–42.4)	88.4 kPa (87.1–89.5)
		B	8.1 kPa (8.0–8.6)	11.2 kPa (11.0–11.4)	43.8 kPa (41.5–45.9)	94.1 kPa (85.7–98.8)
		A + B	7.7 kPa (7.2–8.6)	11.0 kPa (10.8–11.4)	42.0 kPa (41.3–45.9)	89.0 kPa (85.7–98.8)
	Curvilinear	A	6.5 kPa (6.4–6.6)	10.2 kPa (9.9–10.2)	36.5 kPa (35.43–38.0)	63.5 kPa (54.9–72.2)
		B	6.8 kPa (6.6–7.1)	9.8 kPa (9.7–9.9)	36.1 kPa (35.3–37.0)	64.3 kPa (60.4–67.9)
		A + B	6.6 kPa (6.4–7.1)	9.9 kPa (9.7–10.2)	36.2 kPa (35.3–38.0)	64.3 kPa (54.9–72.2)
SSI	Linear	A	7.2 kPa (7.0–7.9)	10.6 kPa (10.3–10.9)	42.8 kPa (40.8–43.6)	84.5 kPa (79.9–92.7)
		B	7.0 kPa (6.9–7.3)	10.3 kPa (10.2–10.4)	42.5 kPa (41.5–43.7)	91.9 kPa (88.4–94.3)
		A + B	7.0 kPa (6.9–7.9)	10.4 kPa (10.2–10.9)	42.6 kPa (40.8–43.7)	89.3 kPa (79.9–94.3)
	Curvilinear	A	11.7 kPa (10–13.5)	15.4 kPa (12.2–18.9)	36.9 kPa (35.0–38.7)	52.9 kPa (49.0–57.2)
		B	10.7 kPa (10.1–11.9)	14.0 kPa (12–15.9)	33.8 kPa (32.5–34.8)	58.9 kPa (52.1–64.7)
		A + B	11.1 kPa (10.0–13.5)	14.5 kPa (12.0–18.9)	34.9 kPa (32.5–38.7)	56.5 kPa (49.0–64.7)
GE-E	Linear	A	0.8 E (0.7–1.1)	0.8 E (0.7–0.8)	1.3 E (1.2–1.4)	2.9 E (2.7–3.2)
		B	0.7 E (0.7–0.7)	0.8 E (0.7–0.9)	1.2 E (1.1–1.3)	1.88 E (1.7–2.0)
		A + B	0.7 E (0.7–1.1)	0.8 E (0.7–0.9)	1.2 E (1.1–1.4)	2.35 E (1.7–3.2)
	Curvilinear	A	0.7 E (0.6–1.0)	0.7 E (0.7–0.7)	1.4 E (1.2–1.6)	2.55 E (2.3–3.0)
		B	0.6 E (0.5–0.6)	0.8 E (0.7–0.9)	1.5 E (1.2–2.1)	2.7 E (2.1–3.0)
		A + B	0.6 E (0.5–1.0)	0.7 E (0.7–0.9)	1.4 E (1.2–2.1)	2.6 E (2.1–3.0)
Hitachi	Linear	A	0.7 SR (0.7–0.8)	0.9 SR (0.8–0.9)	2.3 SR (2.1–2.4)	2.5 SR (2.3–2.7)
		B	0.6 SR (0.6–0.7)	0.8 SR (0.7–0.8)	1.9 SR (1.8–2.0)	2.8 SR (2.5–2.9)
		A + B	0.6 SR (0.6–0.8)	0.9 SR (0.7–0.9)	1.9 SR (1.8–2.4)	2.7 SR (2.3–2.9)
	Curvilinear	A	0.4 SR (0.4–0.5)	0.7 SR (0.6–0.7)	1.3 SR (1.2–1.4)	2.2 SR (2.1–2.2)
		B	0.5 SR (0.5–0.6)	0.7 SR (0.6–0.8)	1.2 SR (1.1–1.3)	2.0 SR (1.9–2.2)
		A + B	0.5 SR (0.4–0.6)	0.67 SR (0.6–0.8)	1.2 SR (1.1–1.4)	2.1 SR (1.9–2.2)

ER = expected elastic ratio.
Background elasticity is 25 ± 6 kPa.
Numbers are mean (min–max) should apply for all numbers

Intra-observer variability analysis revealed higher measurement variability for hard compared with soft inclusions for all systems (Fig. 2a–i). The harder inclusions also exhibited more variation in measurements using curvilinear compared with linear probes for strain-based systems, whereas no significant difference in variability because of probe design could be identified for the SWE systems.

DISCUSSION

In this head-to-head comparison of five elastography software platforms made for clinical scanning and available in commercial scanners, we found that all systems reliably differentiated four inclusions that were softer or harder than the surrounding tissue-mimicking phantom material. In all systems, we found a high level of intra- and inter-observer repeatability. We chose to use the scanner software, as proposed by the makers of the US equipment, to compare data in the same way as intended for clinical application. As strain-based and shear wave-based methods enable different methods for quantification of tissue stiffness, it might be argued that a more stringent comparison between strain- and shear wave-based elastography would be SWE reported as a ratio of Young's modulus (kPa) or shear wave speed (m/s) in background and in inclusions. However, this would not correspond to the measurements of clinical users of the equipment.

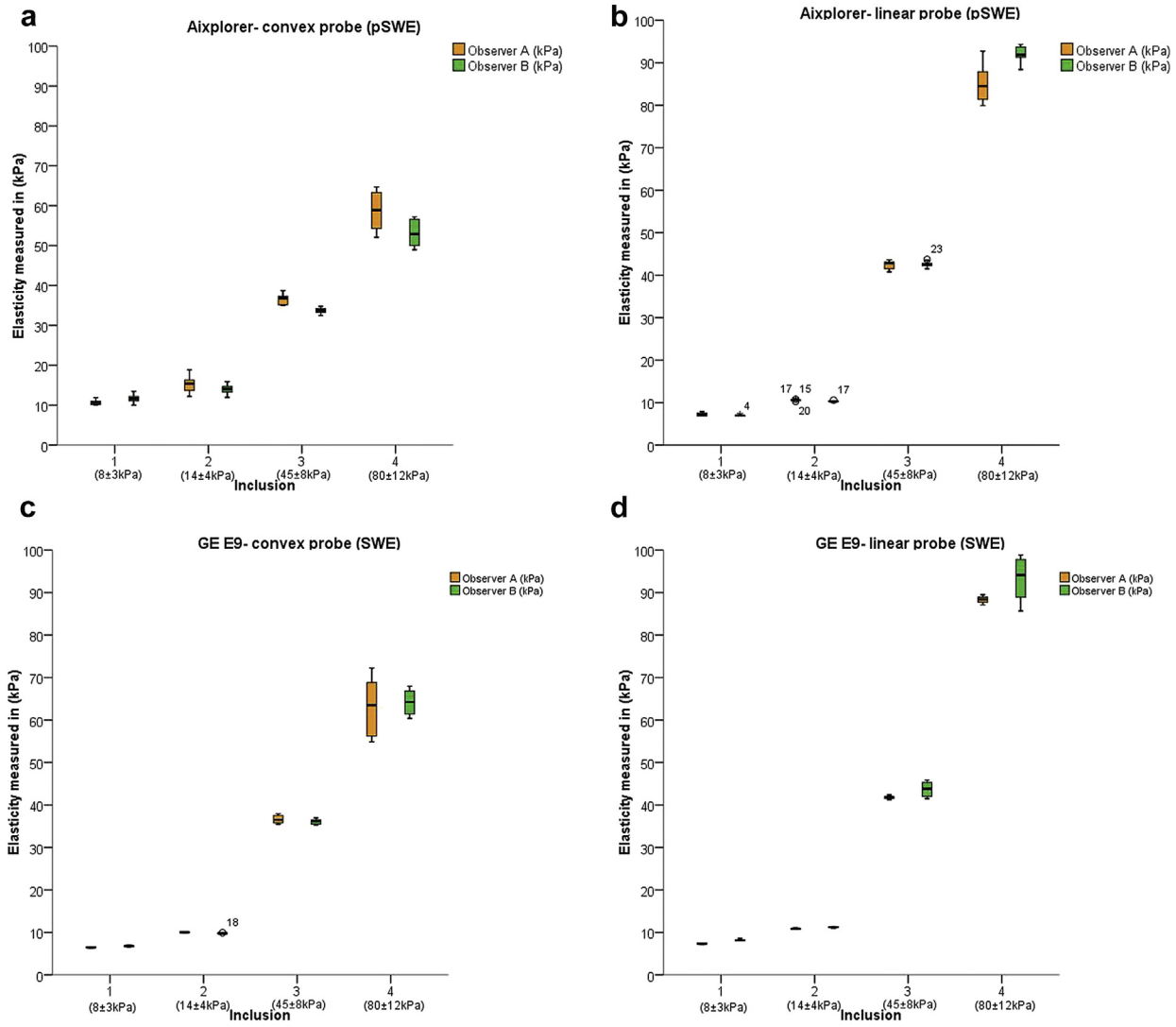

Fig. 2. Variation in elasticity measurements: The boxplot displays the median and 50% percentile (interquartile range); whiskers represent the 90% percentile of the measured elasticity by each the two observers for the four inclusions. The height of the box represents the measurement variability of the single observer for each of the inclusions. The horizontal axis represents the four inclusions with increasing stiffness: inclusion 1 (8 ± 3 kPa), inclusion 2 (14 ± 4 kPa), inclusion 3 (45 ± 8 kPa), inclusion 4 (80 ± 12) in a background of 25 ± 6 kPa. The horizontal axis represents elasticity value (strain ratio/kPa/elasticity). The systems and the applied probes are provided within the figure. SWE = shear wave elastography; pSWE = point SWE; SR = strain ratio.

Generally, the repeatability in quantitative elasticity measurements was lower for the harder inclusions than for the softer inclusions.

In quantification of elasticity in the tissue-mimicking phantom, the two shear wave-based systems SSI and GE-SWE provided elasticity values in kPa closest to the elasticity values provided by the producer of the phantom (Table 2). These two systems also exhibited very high repeatability in elasticity measurements for all four inclusions. SSI and GE-SWE measurements were made based on single cine loops lasting 3–6 s. In contrast, pSWE measurements were made based on 10 individual acquisitions with a cool-down period in between. This might have been anticipated to introduce a bias, as a stable position and pressure might be more difficult to achieve for pSWE; however, this difference would persist also for clinical application of the methods. Furthermore, all the systems evaluated in this study exhibited a high level of repeatability in quantitative elasticity measurements, with ICC values ranging from 0.932 to 1.0 for individual observers and from 0.845 to 0.996 between two observers (Table 3). Significant differences were seen in inter-observer data examining the same inclusions. In one system (GE-SE), the repeatability

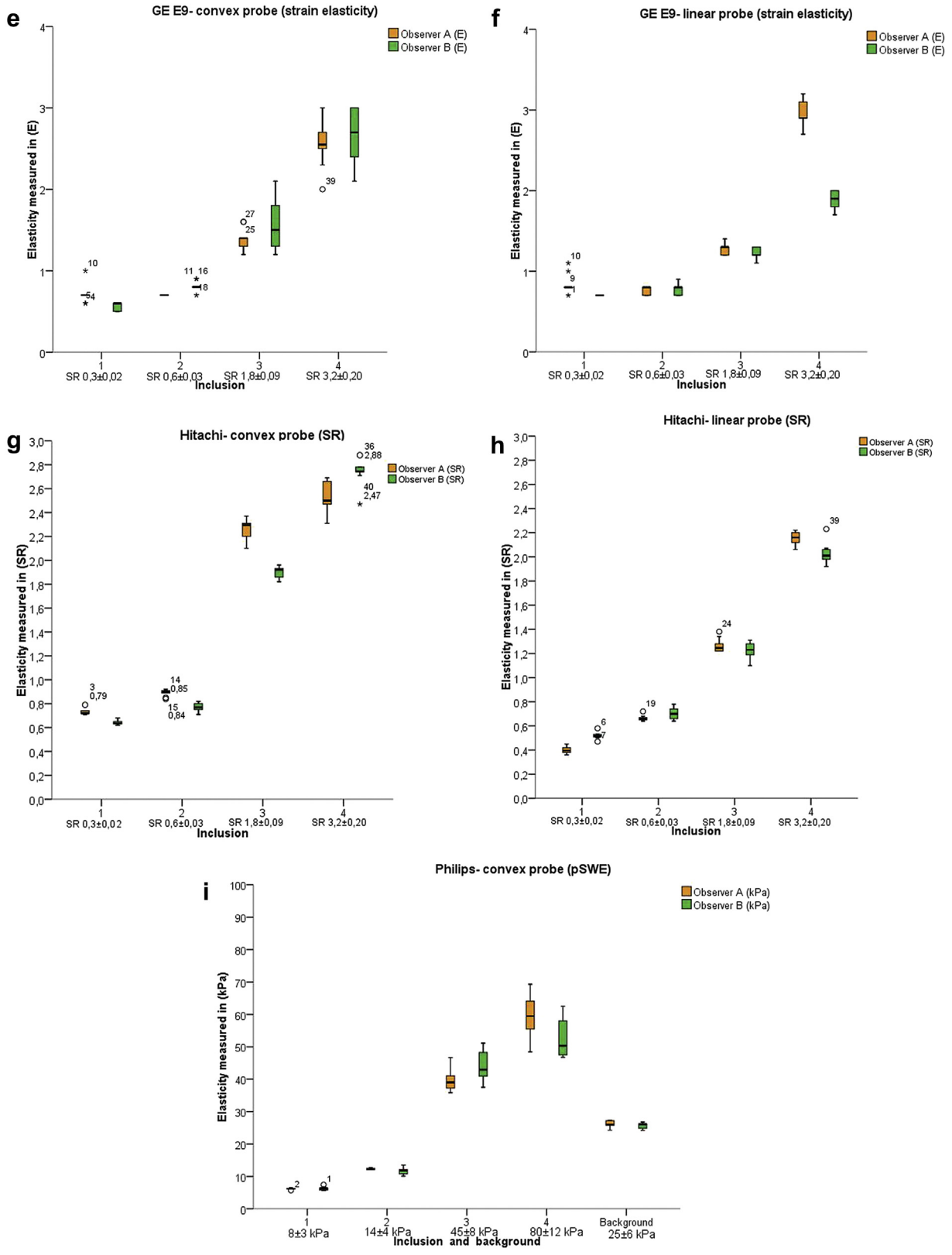

Fig. 2. (*continued*).

Table 3. Measurement repeatability by system, probe and observer

				Mean		Coefficient of variation		Intra-class correlation coefficient		
System	Unit	Probe	Inclusion	A	B	A	B	A	B	AB*
Philips	kPa	C5-1	1	6.2	6.3	0.03	0.09	0.983	0.986	0.975
			2	12.3	11.6	0.02	0.09			
			3	39.5	44.1	0.08	0.1			
			4	59.0	52.3	0.12	0.11			
			Background	26.2	25.7	0.04	0.03			
GE (SWE)	kPa	9 L	1	7.4	8.2	0.02	0.09	1	0.996	0.998
			2	10.9	11.2	0.01	0.01			
			3	41.8	43.7	0.01	0.04			
			4	88.4	93.0	0.01	0.05			
		C1-5	1	6.5	6.8	0.01	0.03	0.986	0.996	0.991
			2	10.2	9.8	0.01	0.01			
			3	36.6	36.1	0.03	0.02			
			4	63.1	64.2	0.11	0.05			
Aixplorer	kPa	L10-2	1	7.3	7.0	0.05	0.02	0.997	1	0.996
			2	10.6	10.4	0.02	0.01			
			3	42.4	42.5	0.02	0.02			
			4	84.9	91.9	0.05	0.02			
		C1-6	1	10.7	11.7	0.06	0.09	0.995	0.99	0.984
			2	15.2	14.1	0.13	0.08			
			3	36.6	33.7	0.04	0.02			
			4	58.7	53.2	0.07	0.06			
GE	(E)	9 L	1	0.8	0.7	0.14	0.00	0.992	0.977	0.845
			2	0.8	0.8	0.07	0.09			
			3	1.3	1.2	0.05	0.06			
			4	3.0	1.9	0.05	0.05			
		C1-5	1	0.7	0.6	0.16	0.09	0.976	0.956	0.964
			2	0.7	0.8	0.00	0.07			
			3	1.4	1.6	0.1	0.19			
			4	2.6	2.7	0.11	0.12			
Hitachi	SR	L-53	1	0.7	0.6	0.03	0.03	0.993	0.998	0.995
			2	0.9	0.8	0.03	0.05			
			3	2.3	1.9	0.03	0.03			
			4	2.5	2.7	0.05	0.04			
		C5-1	1	0.4	0.5	0.07	0.05	0.999	0.995	0.997
			2	0.7	0.7	0.03	0.07			
			3	1.3	1.2	0.04	0.05			
			4	2.2	2.03	0.02	0.04			

* Inter-observer intra-class correlation coefficient.

between two observers was lower when a linear probe was used compared with a curvilinear probe (Fig. 3g–h). In those systems in which both curvilinear and linear probes were available, the measurements made with a curvilinear probe generally had higher intra-observer variability. This finding was expected in the strain-based systems, where movements of the probe were used to generate strain. We anticipated that a linear probe would transfer stress more evenly to the flat surface and underlying material of the phantom than a curved probe surface. One study found bias in SWE in phantoms caused by the probe surface design (Zhao et al. 2011), but no studies have addressed the impact of probe surface design for US strain imaging.

In this study, all platforms were used on the same inclusions in a single phantom with known parameters (Young's modulus, diameter and depth of inclusion), providing stable conditions and eliminating the differences in echogenicity, tissue movement, position, and scanning depth encountered when scanning patients. The phantom represented standardized and simplified conditions for investigating freehand application and allows fair comparison of the methods. We found higher variability in inclusions with lager elastic contrast between inclusion and background (*i.e.,* the harder lesions), in line with previously published studies. Carlsen et al. reported significantly increased variability in harder lesions for strain ratios in a similar phantom. Using acoustic radiation force impulse imaging (Virtual Tissue Quantification) and deformation imaging (Virtual Tissue Imaging) on a Siemens scanner, they found that the diameter of inclusions significantly influenced elastographic measurements (Carlsen et al. 2015). This association might arise in lesions with a smaller area than the fixed pre-set size of the measurement area for shear wave speed (not amendable by the user) in pSWE systems. Previous studies have also reported that shear wave velocity is underestimated with

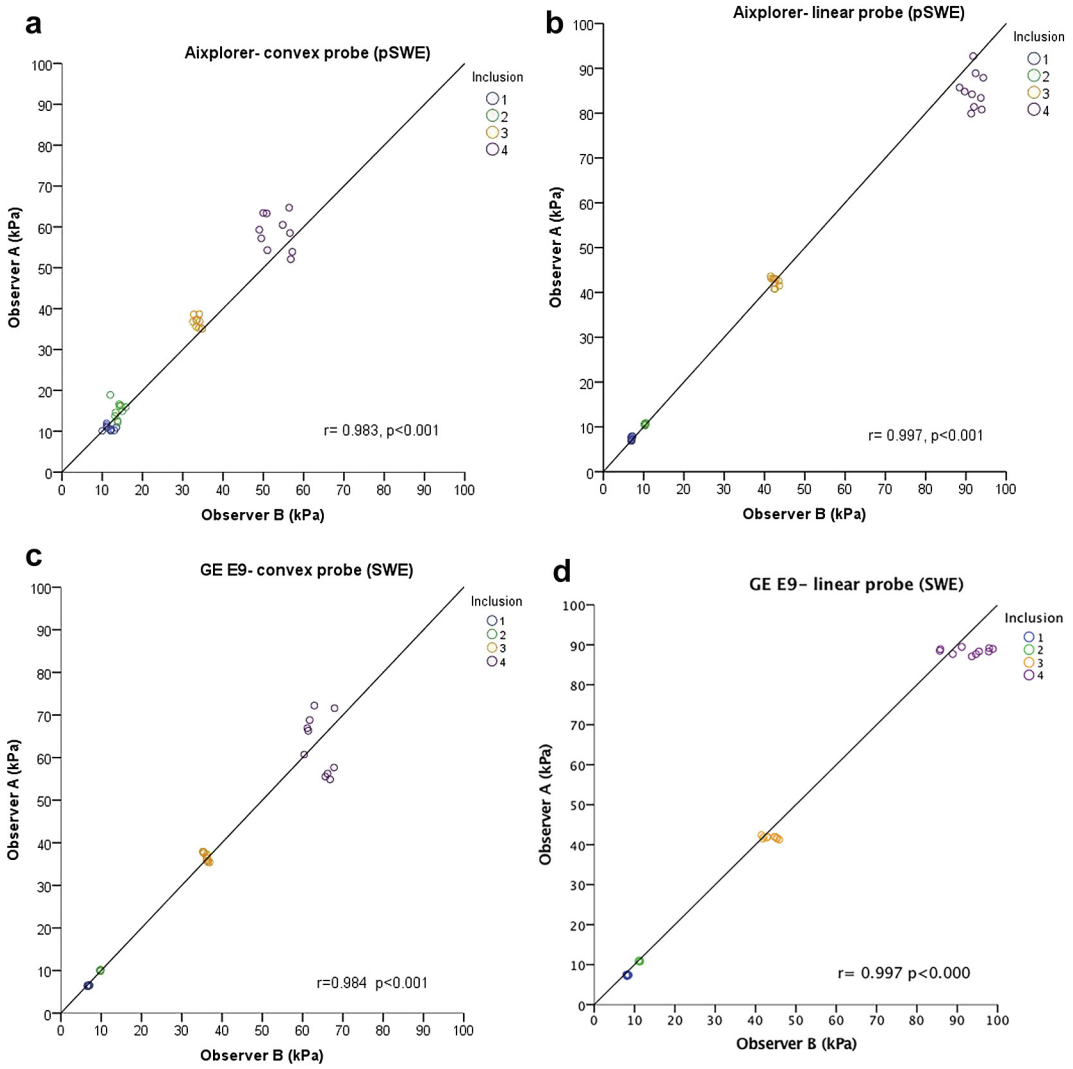

Fig. 3. Correlation between observers for measurements within each lesion: The horizontal and vertical axes represent measurements by observers B and A, respectively. The unit measured is strain ratio/kPa/elasticity depending on the elasticity platform used. The line in the graph represents the line of unity. The colors represent the different inclusions: *blue* = inclusion 1 (8 ± 3 kPa); *green* = inclusion 2 (14 ± 4 kPa); *orange* = inclusion 3 (45 ± 8 kPa); *purple* = inclusion 4 (80 ± 12); *black* = background (25 ± 6 kPa). The Pearson correlation coefficient (r) and significance (p) are given in the top right corner. SWE = shear wave elastography; pSWE = point SWE; SR = strain ratio.

increasing focal depth (Tozaki et al. 2011; Yamanaka et al. 2012), whereas Carlsen et al. reported that significant decrease in shear wave velocity was restricted to hard inclusions placed deep in the phantom. For SSI, several phantom validation studies have been published, reporting good intra- and inter-observer reproducibility similar to our results in the present study (Ramnarine et al. 2014), and with slightly lower intra-observer reproducibility by ICC with a higher number of compared observers and number of repeated examinations. Mun et al. (2013) found an inter-observer ICC of 0.82 for mean elasticity using SSI on a breast phantom with 12 inclusions between four observers. With a larger number of observations compared, the expected reproducibility would be lower than in our study. A comparison between four different quantitative elastography techniques in Zerdine phantoms was presented by Oudry et al. (2014). Transient elastography was compared with mechanical testing, large-range quasi-static elastography and hyper-frequency viscoelastic spectroscopy, where only transient elastography is available in a clinical scanner. The authors concluded that as a result of different phantom geometry, pre-compression and shear wave frequency, it was hard to define a gold standard for quantitative elastography based on the available data

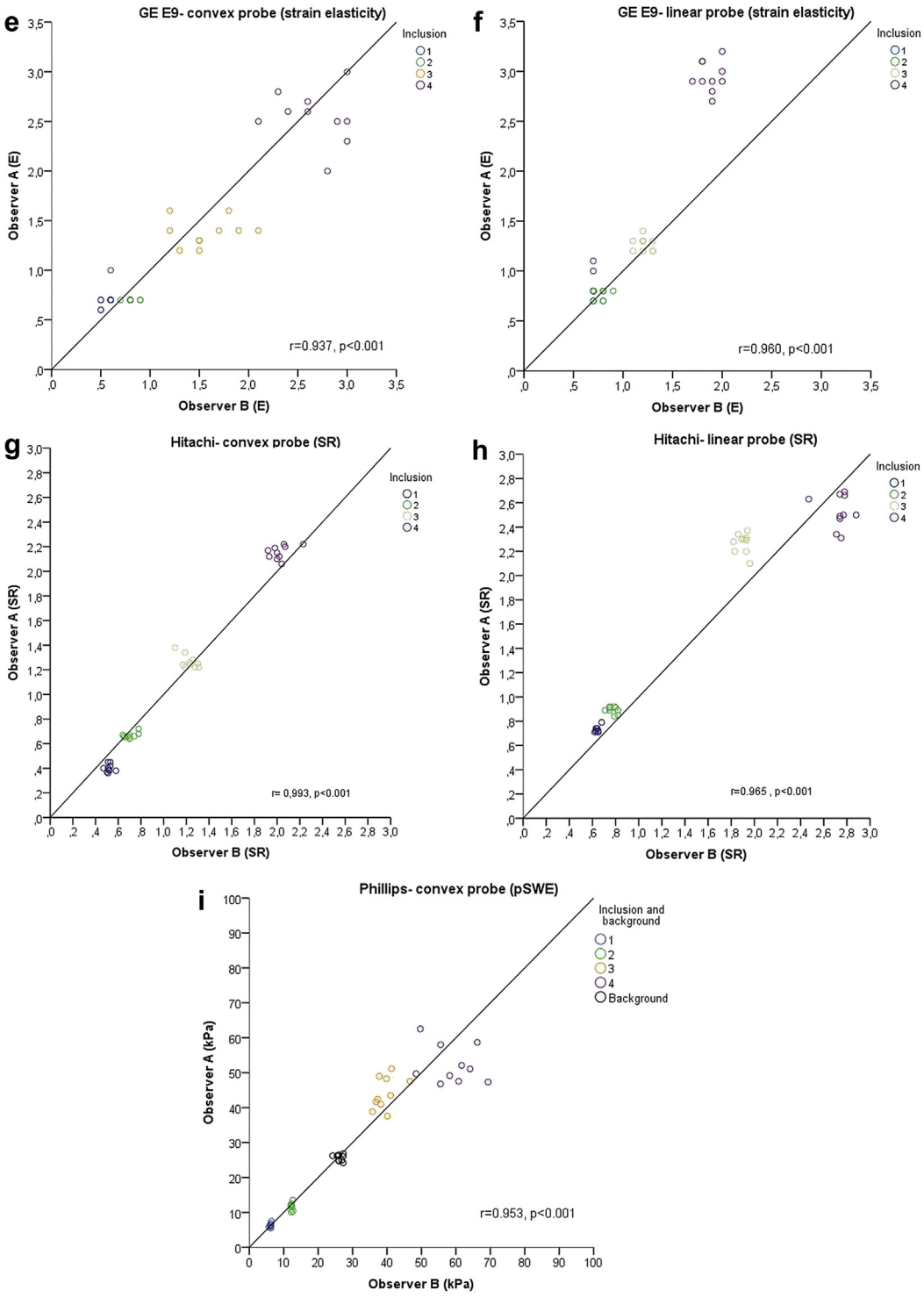

Fig. 3. (*continued*).

(Oudry et al. 2014). The mean bias of expected SWE measurements for all inclusions was in the range −0.02 to −0.21 for SWE systems and probes (Table 4). It has also been reported that the frequency and shear wave speed are influenced by the viscosity and geometry of soft tissue and, thus, the shear wave-derived elasticity (Chen et al. 2004, 2009; Nenadic et al. 2011). Factors such as phantom geometry and pre-compression may influence elasticity imaging and measurements, and we sought to minimize this in our

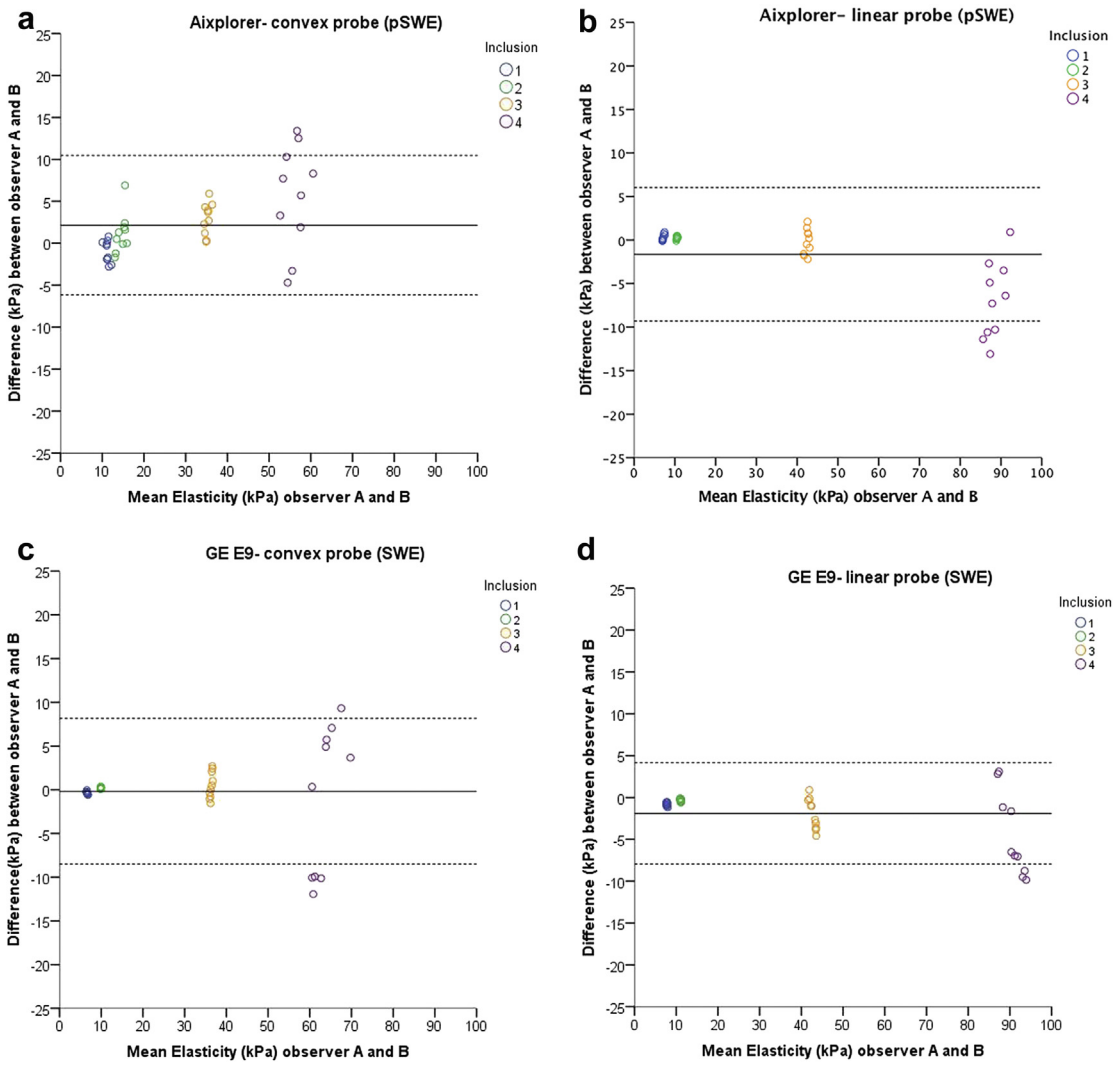

Fig. 4. Limits of agreement: variation and agreement for two observers' measurements. The horizontal axis represents the common mean value of all measurements for both observers, whereas the vertical axis represents the difference between individual measurements and this common mean (strain ratio/kPa/elasticity), displaying the variability of measurements for the four inclusions. The *black line* represents the common mean value; the *dotted lines* represent standard deviation × 2 (≈95% confidence interval). A mean value close to 0 on the vertical axis indicates that the two observers applied the measurement scale without bias. If the mean value deviates from 0, one of the observers tended to measure higher or lower values systematically compared with the other observer.

study by selecting reference tissue not too close to phantom encasement or surface and by minimizing precompression in a freehand setting.

The development of elastography has been a major advantage in the clinical assessment of predicting the stage of liver fibrosis, and high diagnostic accuracy has been reported (Ferraioli et al. 2012a, 2012b; Friedrich-Rust et al. 2008; Sporea et al. 2012a, 2012b). We found very high reproducibility in repeated examinations of material stiffness in four selected inclusions, higher than for most clinically used imaging methods. The variance seen in clinical examinations, however, is most probably higher because of patient-related factors and a much more complex structure in live tissue. Clinical users of US elastography have been introduced to a number of new parameters for quantification of strain or tissue elasticity over the past 10 y (Castera et al. 2008; Piscaglia et al. 2014). From our results in this study, combined with experience in clinical elastography scanning, use of a log scale for elasticity parameters seems interesting. A log scale would maintain the representation of low numerical values, for example, in soft lesions, while the higher values found in stiffer lesions would be perceived with lower measurement variability. This would perhaps facilitate measurement reproducibility

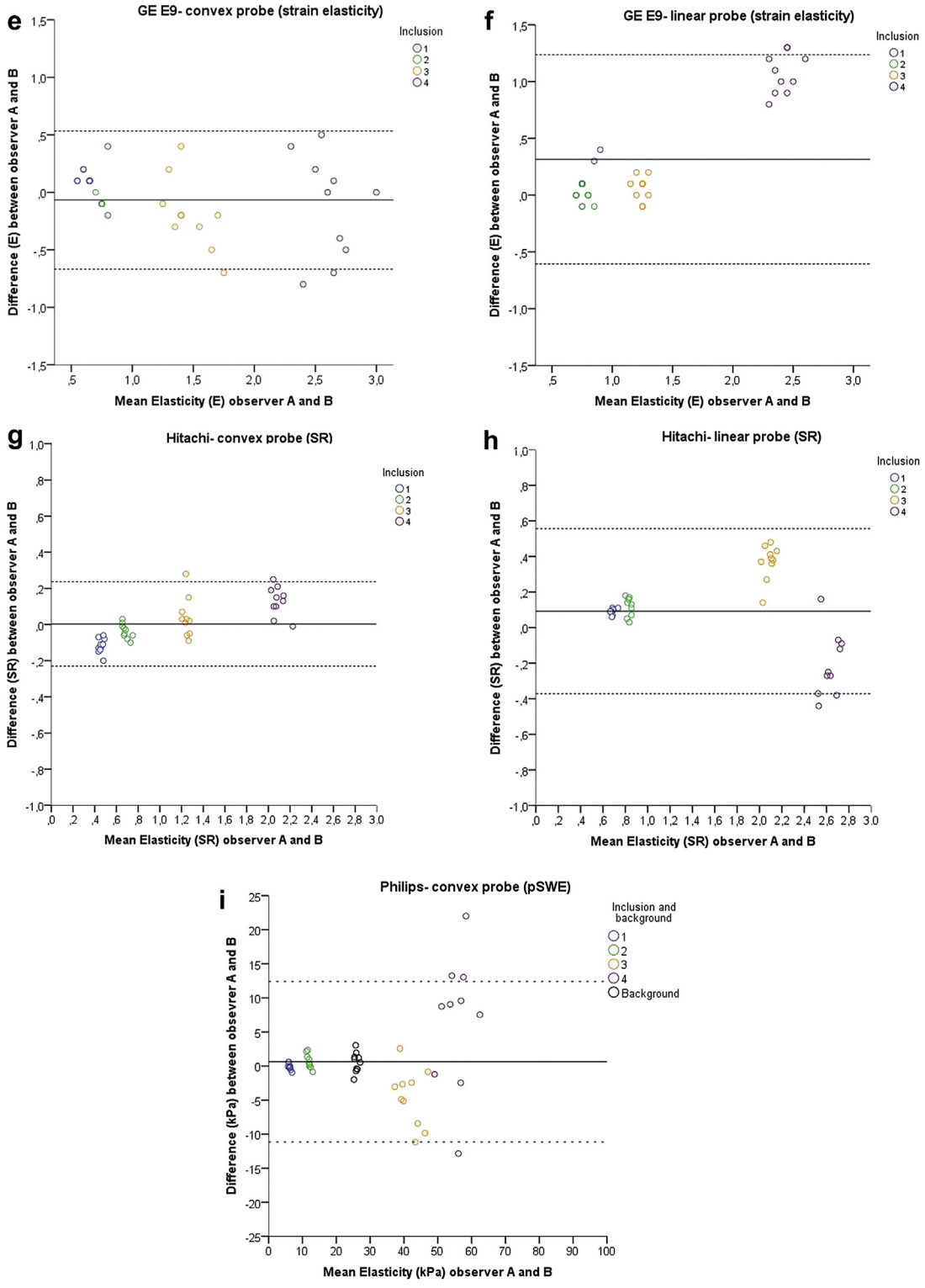

Fig. 4. (*continued*).

Table 4. Bias of measurements in SWE systems

System	Probe	Inclusion	Pooled mean (kPa)	Expected Young's modulus (kPa)	Bias
Philips	C5-1	1	6.3	8	−0.22
		2	11.9	14	−0.15
		3	41.8	45	−0.07
		4	55.7	80	−0.30
		Background	25.9	25	0.04
GE (SWE)	9 L	1	7.8	8	−0.03
		2	11.1	14	−0.21
		3	42.8	45	−0.05
		4	90.7	80	0.13
	C1-5	1	6.7	8	−0.17
		2	10.0	14	−0.29
		3	36.4	45	−0.19
		4	63.7	80	−0.20
Aixplorer	L10-2	1	7.2	8	−0.11
		2	10.5	14	−0.25
		3	42.5	45	−0.06
		4	88.4	80	0.11
	C1-6	1	11.2	8	0.40
		2	14.7	14	0.05
		3	35.2	45	−0.22
		4	55.9	80	−0.30

SWE = shear wave elastography.

and yield numerical data for more robust cutoff values in clinical settings.

The observers had different levels of experience in performing ultrasound elastography; one of the observers had less experience than the two other observers. None of the observers were familiar or experienced with all of the systems. Previous reports indicate that training and experience should be taken into account when examining liver stiffness with SWE (Ferraioli et al. 2014), whereas strain imaging reported as SR did not seem affected by operator experience in one recent phantom study (Carlsen et al. 2014). Our results suggest that in a simplified model of scanning a tissue-mimicking phantom, the learning curve in elastography is steeper than that in scanning liver tissue. No data from a single observer were discarded in any of the platforms.

Limitations of the study

This *in vitro* study has several important limitations and simplifications. The US phantom did not provide viscoelastic properties like live soft tissues. The study design allowed evaluation and comparison of the reproducibility of the methods under idealized conditions, and the results cannot be immediately transferred to a complex clinical setting. To evaluate reproducibility in live tissue, further studies are needed. The probes used in this study had minor differences in shape and US frequency in the range 1–10 MHz. Because of the different elastography methods applied (pSWE/SWE and SE), the ROI was not identical for all systems. Not all shear wave methods provided both shear wave speed and kilopascal measurements at the same time. This had to be preselected in one of the platforms.

CONCLUSIONS

Using five different platforms, we had good to excellent repeatability of elasticity or strain measurements in four focal inclusions in a tissue-mimicking phantom. The repeatability for intra- and inter-observations exhibited excellent ICC and VC values for the systems tested. For soft inclusions, the systems had very high repeatability and low inter-observer variations. The shear wave-based elastography methods SSI and GE-SWE produced elasticity measurements closest to the values provided by the producer of the phantom. Freehand real-time strain measurements also exhibited excellent intra-observer variability, but with some variability between observers. These results confirm a high level of repeatability for all tested elastography platforms in an *in vitro* setting, but further studies are needed to evaluate clinical applications.

Acknowledgments—The study was supported by MedViz, an interdisciplinary research cluster from Haukeland University Hospital, University of Bergen and Christian Michelsen Research AS. We express our gratitude to BBS Medical AB, Sweden, and GE Healthcare for providing scanners and software. We thank Dieter Maier, Sales Manager, and Joel Gay, Clinical Manager, at SuperSonic Imagine for valuable information and Ted Lynch, Manager, Engineering and Product Development, at CIRS Inc. We also thank Michael Wang, System Engineer, at GE Healthcare for valuable information on the GE-SWE platform before this was released.

SUPPLEMENTARY DATA

Supplementary data related to this article can be found at http://dx.doi.org/10.1016/j.ultrasmedbio.2016.07.002.

REFERENCES

Bamber J, Cosgrove D, Dietrich CF, Fromageau J, Bojunga J, Calliada F, Cantisani V, Correas JM, D'Onofrio M, Drakonaki EE, Fink M, Friedrich-Rust M, Gilja OH, Havre RF, Jenssen C, Klauser AS, Ohlinger R, Saftoiu A, Schaefer F, Sporea I, Piscaglia F. EFSUMB guidelines and recommendations on the clinical use of ultrasound elastography: Part 1. Basic principles and technology. Ultraschall Med 2013;34:169–184.

Bercoff J, Tanter M, Fink M. Supersonic shear imaging: A new technique for soft tissue elasticity mapping. IEEE Trans Ultrason Ferroelectr Freq Control 2004;51:396–409.

Bhatia KS, Tong CS, Cho CC, Yuen EH, Lee YY, Ahuja AT. Shear wave elastography of thyroid nodules in routine clinical practice: Preliminary observations and utility for detecting malignancy. Eur Radiol 2012;22:2397–2406.

Bland JM, Altman DG. Measuring agreement in method comparison studies. Stat Methods Med Res 1999;8:135–160.

Bland JM, Altman DG. Agreement between methods of measurement with multiple observations per individual. J Biopharm Stat 2007;17:571–582.

Browne JE, Ramnarine KV, Watson AJ, Hoskins PR. Assessment of the acoustic properties of common tissue-mimicking test phantoms. Ultrasound Med Biol 2003;29:1053–1060.

Carlsen JF, Ewertsen C, Saftoiu A, Lonn L, Nielsen MB. Accuracy of visual scoring and semi-quantification of ultrasound strain elastography—A phantom study. PloS One 2014;9:e88699.

Carlsen JF, Pedersen MR, Ewertsen C, Saftoiu A, Lonn L, Rafaelsen SR, Nielsen MB. A comparative study of strain and shear-wave elastography in an elasticity phantom. AJR Am J Roentgenol 2015;204: W236–W242.

Cassinotto C, Lapuyade B, Mouries A, Hiriart JB, Vergniol J, Gaye D, Castain C, Le Bail B, Chermak F, Foucher J, Laurent F, Montaudon M, De Ledinghen V. Non-invasive assessment of liver fibrosis with impulse elastography: Comparison of supersonic shear imaging with ARFI and FibroScan(R). J Hepatol 2014;61:550–557.

Castera L, Forns X, Alberti A. Non-invasive evaluation of liver fibrosis using transient elastography. J Hepatol 2008;48:835–847.

Chen S, Fatemi M, Greenleaf JF. Quantifying elasticity and viscosity from measurement of shear wave speed dispersion. J Acoust Soc Am 2004;115:2781–2785.

Chen S, Urban MW, Pislaru C, Kinnick R, Zheng Y, Yao A, Greenleaf JF. Shearwave dispersion ultrasound vibrometry (SDUV) for measuring tissue elasticity and viscosity. IEEE Trans Ultrason Ferroelectr Freq Control 2009;56:55–62.

Cho N, Moon WK, Kim HY, Chang JM, Park SH, Lyou CY. Sonoelastographic strain index for differentiation of benign and malignant nonpalpable breast masses. J Ultrasound Med 2010;29:1–7.

D'Onofrio M, De Robertis R, Crosara S, Poli C, Canestrini S, Demozzi E, Pozzi Mucelli R. Acoustic radiation force impulse with shear wave speed quantification of pancreatic masses: A prospective study. Pancreatology 2016;16:106–109.

Deffieux T, Montaldo G, Tanter M, Fink M. Shear wave spectroscopy for *in vivo* quantification of human soft tissues visco-elasticity. IEEE Trans Med Imaging 2009;28:313–322.

Dillman JR, Chen S, Davenport MS, Zhao H, Urban MW, Song P, Watcharotone K, Carson PL. Superficial ultrasound shear wave speed measurements in soft and hard elasticity phantoms: Repeatability and reproducibility using two ultrasound systems. Pediatr Radiol 2015;45:376–385.

Ferraioli G, Tinelli C, Dal Bello B, Zicchetti M, Filice G, Filice C, Liver Fibrosis Study Group. Accuracy of real-time shear wave elastography for assessing liver fibrosis in chronic hepatitis C: A pilot study. Hepatology 2012a;56:2125–2133.

Ferraioli G, Tinelli C, Lissandrin R, Zicchetti M, Bernuzzi S, Salvaneschi L, Filice C. Elastography Study Group. Ultrasound point shear wave elastography assessment of liver and spleen stiffness: Effect of training on repeatability of measurements. Eur Radiol 2014;24:1283–1289.

Ferraioli G, Tinelli C, Zicchetti M, Above E, Poma G, Di Gregorio M, Filice C. Reproducibility of real-time shear wave elastography in the evaluation of liver elasticity. Eur J Radiol 2012b;81:3102–3106.

Franchi-Abella S, Elie C, Correas JM. Ultrasound elastography: advantages, limitations and artefacts of the different techniques from a study on a phantom. Diagn Interv Imaging 2013;94: 497–501.

Fraquelli M, Rigamonti C, Casazza G, Conte D, Donato MF, Ronchi G, Colombo M. Reproducibility of transient elastography in the evaluation of liver fibrosis in patients with chronic liver disease. Gut 2007; 56:968–973.

Friedrich-Rust M, Ong MF, Martens S, Sarrazin C, Bojunga J, Zeuzem S, Herrmann E. Performance of transient elastography for the staging of liver fibrosis: A meta-analysis. Gastroenterology 2008;134:960–974.

Friedrich-Rust M, Vorlaender C, Dietrich CF, Kratzer W, Blank W, Schuler A, Broja N, Cui XW, Herrmann E, Bojunga J. Evaluation of strain elastography for differentiation of thyroid nodules: Results of a prospective DEGUM multicenter study. Ultraschall Med 2016; 37:262–270.

Garra BS, Cespedes EI, Ophir J, Spratt SR, Zuurbier RA, Magnant CM, Pennanen MF. Elastography of breast lesions: Initial clinical results. Radiology 1997;202:79–86.

Gennisson JL, Deffieux T, Mace E, Montaldo G, Fink M, Tanter M. Viscoelastic and anisotropic mechanical properties of *in vivo* muscle tissue assessed by supersonic shear imaging. Ultrasound Med Biol 2010;36:789–801.

Giovannini M, Thomas B, Erwan B, Christian P, Fabrice C, Benjamin E, Genevieve M, Paolo A, Pierre D, Robert Y, Walter S, Hanz S, Carl S, Christoph D, Pierre E, Jean-Luc VL, Jacques D, Peter V, Andrian S. Endoscopic ultrasound elastography for evaluation of lymph nodes and pancreatic masses: a multicenter study. World J Gastroenterol 2009;15:1587–1593.

Havre RF, Odegaard S, Gilja OH, Nesje LB. Characterization of solid focal pancreatic lesions using endoscopic ultrasonography with real-time elastography. Scand J Gastroenterol 2014;49:742–751.

Itoh A, Ueno E, Tohno E, Kamma H, Takahashi H, Shiina T, Yamakawa M, Matsumura T. Breast disease: Clinical application of US elastography for diagnosis. Radiology 2006;239:341–350.

Itokawa F, Itoi T, Sofuni A, Kurihara T, Tsuchiya T, Ishii K, Tsuji S, Ikeuchi N, Umeda J, Tanaka R, Yokoyama N, Moriyasu F, Kasuya K, Nagao T, Kamisawa T, Tsuchida A. EUS elastography combined with the strain ratio of tissue elasticity for diagnosis of solid pancreatic masses. J Gastroenterol 2011;46:843–853.

Janssen J, Dietrich CF, Will U, Greiner L. Endosonographic elastography in the diagnosis of mediastinal lymph nodes. Endoscopy 2007;39:952–957.

Janssen J, Papavassiliou I. Effect of aging and diffuse chronic pancreatitis on pancreas elasticity evaluated using semiquantitative EUS elastography. Ultraschall Med 2014;35:253–258.

Mei M, Ni J, Liu D, Jin P, Sun L. EUS elastography for diagnosis of solid pancreatic masses: a meta-analysis. Gastrointest Endosc 2013;77: 578–589.

Mun HS, Choi SH, Kook SH, Choi Y, Jeong WK, Kim Y. Validation of intra- and interobserver reproducibility of shearwave elastography: Phantom study. Ultrasonics 2013;53:1039–1043.

Nenadic IZ, Urban MW, Mitchell SA, Greenleaf JF. Lamb wave dispersion ultrasound vibrometry (LDUV) method for quantifying mechanical properties of viscoelastic solids. Phys Med Biol 2011;56: 2245–2264.

Oudry J, Lynch T, Vappou J, Sandrin L, Miette V. Comparison of four different techniques to evaluate the elastic properties of phantom in elastography: Is there a gold standard? Phys Med Biol 2014;59: 5775–5793.

Palmeri ML, Frinkley KD, Zhai L, Gottfried M, Bentley RC, Ludwig K, Nightingale KR. Acoustic radiation force impulse (ARFI) imaging of the gastrointestinal tract. Ultrason Imaging 2005a;27:75–88.

Palmeri ML, Sharma AC, Bouchard RR, Nightingale RW, Nightingale KR. A finite-element method model of soft tissue response to impulsive acoustic radiation force. IEEE Trans Ultrason Ferroelectr Freq Control 2005b;52:1699–1712.

Piscaglia F, Marinelli S, Bota S, Serra C, Venerandi L, Leoni S, Salvatore V. The role of ultrasound elastographic techniques in chronic liver disease: Current status and future perspectives. Eur J Radiol 2014;83:450–455.

Pozzi E, Mantica G, Gastaldi C, Berardinelli M, Choussos D, Bianchi CM, Roggia A. The role of the elastography in the diagnosis of prostate cancer: A retrospective study on 460 patients. Arch Ital Urol Androl 2012;84:151–154.

Ramnarine KV, Garrard JW, Dexter K, Nduwayo S, Panerai RB, Robinson TG. Shear wave elastography assessment of carotid plaque stiffness: *In vitro* reproducibility study. Ultrasound Med Biol 2014;40:200–209.

Saftoiu A, Vilmann P, Gorunescu F, Gheonea DI, Gorunescu M, Ciurea T, Popescu GL, Iordache A, Hassan H, Iordache S. Neural network analysis of dynamic sequences of EUS elastography used for the differential diagnosis of chronic pancreatitis and pancreatic cancer. Gastrointest Endosc 2008;68:1086–1094.

Salomon G, Kollerman J, Thederan I, Chun FK, Budaus L, Schlomm T, Isbarn H, Heinzer H, Huland H, Graefen M. Evaluation of prostate cancer detection with ultrasound real-time elastography: A comparison with step section pathological analysis after radical prostatectomy. Eur Urol 2008;54:1354–1362.

Sebag F, Vaillant-Lombard J, Berbis J, Griset V, Henry JF, Petit P, Oliver C. Shear wave elastography: A new ultrasound imaging

mode for the differential diagnosis of benign and malignant thyroid nodules. J Clin Endocrinol Metab 2010;95:5281–5288.

Shin HJ, Kim MJ, Kim HY, Roh YH, Lee MJ. Comparison of shear wave velocities on ultrasound elastography between different machines, transducers, and acquisition depths: A phantom study. Eur Radiol 2016 [Epub ahead of print].

Sporea I, Bota S, Peck-Radosavljevic M, Sirli R, Tanaka H, Iijima H, Badea R, Lupsor M, Fierbinteanu-Braticevici C, Petrisor A, Saito H, Ebinuma H, Friedrich-Rust M, Sarrazin C, Takahashi H, Ono N, Piscaglia F, Borghi A, D'Onofrio M, Gallotti A, Ferlitsch A, Popescu A, Danila M. Acoustic radiation force impulse elastography for fibrosis evaluation in patients with chronic hepatitis C: An international multicenter study. Eur J Radiol 2012a;81: 4112–4118.

Sporea I, Sirli R, Bota S, Vlad M, Popescu A, Zosin I. ARFI elastography for the evaluation of diffuse thyroid gland pathology: Preliminary results. World J Radiol 2012b;4:174–178.

Tanter M, Bercoff J, Athanasiou A, Deffieux T, Gennisson JL, Montaldo G, Muller M, Tardivon A, Fink M. Quantitative assessment of breast lesion viscoelasticity: Initial clinical results using supersonic shear imaging. Ultrasound Med Biol 2008;34:1373–1386.

Tozaki M, Saito M, Joo C, Yamaguchi M, Isobe S, Ogawa Y, Homma K, Fukuma E. Ultrasonographic tissue quantification of the breast using acoustic radiation force impulse technology: Phantom study and clinical application. Jpn J Radiol 2011;29:598–603.

Tsutsumi M, Miyagawa T, Matsumura T, Kawazoe N, Ishikawa S, Shimokama T, Shiina T, Miyanaga N, Akaza H. The impact of real-time tissue elasticity imaging (elastography) on the detection of prostate cancer: Clinicopathological analysis. Int J Clin Oncol 2007;12:250–255.

Yamanaka N, Kaminuma C, Taketomi-Takahashi A, Tsushima Y. Reliable measurement by Virtual Touch tissue quantification with acoustic radiation force impulse imaging: phantom study. J Ultrasound Med 2012;31:1239–1244.

Ying L, Lin X, Xie ZL, Tang FY, Hu YP, Shi KQ. Clinical utility of acoustic radiation force impulse imaging for identification of malignant liver lesions: A meta-analysis. Eur Radiol 2012;22: 2798–2805.

Zhao H, Song P, Urban MW, Kinnick RR, Yin M, Greenleaf JF, Chen S. Bias observed in time-of-flight shear wave speed measurements using radiation force of a focused ultrasound beam. Ultrasound Med Biol 2011;37:1884–1892.

Zhi H, Ou B, Luo BM, Feng X, Wen YL, Yang HY. Comparison of ultrasound elastography, mammography, and sonography in the diagnosis of solid breast lesions. J Ultrasound Med 2007;26: 807–815.